Journal of Materials Science and Chemical Engineering, 2017, 5, 12-25
http://www.scirp.org/journal/msce
ISSN Online: 2327-6053
ISSN Print: 2327-6045

Synthesis of CuO_x/MnO_2 Heterostructures with Enhanced Visible Light-Driven Photocatalytic Activity

Tao Yu[1,2], Yangang Sun[2*], Cui Zhe[2], Wei Wang[1#], Pinhua Rao[2†]

[1]School of Materials Engineering, Shanghai University of Engineering Science, Shanghai, China
[2]College of Chemistry and Chemical Engineering, Shanghai University of Engineering Science, Shanghai, China
Email: *syg021@sues.edu.cn, #wangwei200173@sina.com, †raopinhua@hotmail.com

How to cite this paper: Yu, T., Sun, Y.G., Zhe, C., Wang, W. and Rao, P.H. (2017) Synthesis of CuO_x/MnO_2 Heterostructures with Enhanced Visible Light-Driven Photocatalytic Activity. *Journal of Materials Science and Chemical Engineering*, **5**, 12-25.
https://doi.org/10.4236/msce.2017.510002

Received: September 22, 2017
Accepted: October 24, 2017
Published: October 27, 2017

Abstract

Organic pollutants coming from various industry processes are harmful to the environment, and semiconductor heterostructure is a promising candidate catalyst for poisonous wastewater treatment in the future. In this study, CuO_x/MnO_2 heterostructures were successfully constructed, using a facile and effective hydrothermal method and chemical both/calcination route, which exhibited higher photocatalytic activity towards the photodegradation of organic contaminants under visible-light driven irradiation. The resulting CuO_x/MnO_2 heterostructures were systematically characterized using various microscopic and spectroscopic techniques. Morphological characterizations show that the CuO_x nanoparticles are well anchored on the surface of the MnO_2 nanowires (NMs). The photocatalytic activity enhancement of the CuO_x/MnO_2 heterostructures (M-4) could be ascribed to the introduction of CuO_x on the surface of MnO_2 NWs and the efficient separation of the electron-hole pairs compared to other CuO_x/MnO_2 heterostructures and pure MnO_2 NMs. These results show that CuO_x/MnO_2 heterostructures can be a suitable candidate for efficient visible light photocatalysts.

Keywords

CuO_x/MnO_2 Heterostructures, Hydrothermal Method, Chemical Both/Calcination Route, Photocatalytic Activity

1. Introduction

Organic pollutants coming from various processes in industries are harmful to the environment, hazardous to human health due to their toxicity and persistence [1] [2], which has aroused great concern worldwide. Many treatment approaches

have been investigated for the removal of organic pollutants from wastewater including adsorption, chemical oxidation, biological degradation, ultrasound degradation and photocatalytic degradation [3]. Among them, photochemical degradation has been commonly suggested as a cost effective method for the degradation of many toxic organic pollutants from aqueous systems because of its low cost, simplicity and high efficiency [4] [5]. It is a universally acknowledged truth that the high performance catalysts play important roles in photocatalytic degradation application [6] [7]. Thus, designing and developing the high performance catalysts should be a key point to solve organic pollution in wastewater.

As a promising photocatalyst, manganese dioxide (MnO_2) has attracted intensive interest due to its mass of merits like low-cost, environmental compatibility, abundant availability, strong adsorption and oxidation ability [8]-[15]. But the photocatalytic activity of MnO_2 is still restricted by the slow rate of charge transfer and high recombination probability of photogenerated electron-hole pairs. Many efforts have been made to improve the photocatalytic capability of MnO_2, a large number of studies showed that MnO_2 combined with the conductor or semiconductor can effectively improve the photocatalytic activity compared to pure nanostructures. For example, Saravanakumar *et al*. [16] constructed Ag@MnO_2 nanowires, using a one step hydrothermal method, which exhibited excellent efficiency towards the photodegradation of organic contaminants under visible-light driven irradiation compared to pure MnO_2. Zheng *et al*. [17] obtained hybrid 3D Co_3O_4@MnO_2 heterostructures by a facile and highly efficient solution-based method on nickel foam, and the as-synthesized 3D Co_3O_4@MnO_2 heterostructures exhibited remarkable photocatalytic activity and recycling stability for the degradation of organic dyes. A flower-like MnO_2/BiOI composite [18] has been fabricated by a simple and cost-effective approach and demonstrated a photocatalytic degradation efficiency of 97.8% under visible light and 93.4% under simulated solar light irradiation for methyl orange (MO) within 40 min.

We noted that copper oxides as a photocatalyst hold great potential due to their unique optical and charge transport properties [19] [20] [21] [22]. Cu_2O and CuO both are suitable for visible light absorption because of their favorable bandgap values that range from 1.7 to 2.6 eV [23] [24]. On the other hand, Zhou *et al*. [25] and Chen *et al*. [26] separately reported excellent photocatalytic activity of Cu_2O/Cu nanocomposites and Cu/Cu_2O core-shell nanowires for dye degradations of MO and methylene blue (MB).

Inspired by these previous reports, here we have synthesized CuO_x nanoparticle/MnO_2 nanowire heterostructures, via a hydrothermal method followed by a facile and effective chemical both/calcination route. The photocatalytic activity of the CuO_x/MnO_2 nanowire heterostructures was investigated under the irradiation of visible light, and they displayed high performance and stability for the photodecomposition of MB.

2. Experimental Section

2.1. Synthesis of MnO_2 Nanowires

All of the chemicals were of analytical purity and used as received without further purification. MnO_2 nanowires (NWs) were prepared by a simple hydrothermal method. Firstly, the 1.715 g $KMnO_4$ was dissolved in 25 mL of deionized water under magnetic stirring, and 2.5 mL concentrated HCl was added dropwise into the above solution. The mixture of the solution was stirred continuously for 1 h. Secondly, the mixed solution was transferred into a 50 mL Teflon-lined stainless steel autoclave and heated in an oven at 180˚C for 12 h. After the reaction, the autoclave was cooled down to room temperature in air, the sample was then collected by filtration and washed with ethanol and deionized water several times, and dried at 80˚C for 3 h. Finally, the dried sample was further calcined at 500˚C for 1 hour under N_2 environment, and MnO_2 NWs were obtained.

2.2. Synthesis of CuO_x/MnO_2 Heterostructures

CuO_x/MnO_2 heterostructures were synthesized by a simple chemical both and calcination method. Firstly, the 0.174 g of the obtained MnO_2 NWs were dispersed in 50 mL deionized water followed by stirring for 10 min, then 0.72 g of glucose was dissolved in the above solution under the same conditions, 0.2 g of $Cu(AC)_2{\cdot}H_2O$ was added to the mixed solution of MnO_2 NWs and glucose while keeping stirring for 10 min, then the obtained mixed solution was heated in water-bath for 1 hours at 90˚C. Secondly, the product was collected and washed by filtration at room temperature, and dried at 50˚C overnight. Thirdly, the collected solid powders were put into a tubular furnace and heated to 500˚C at a rate of $5^{\circ}C{\cdot}min^{-1}$ and maintained for 180 min under N_2 protection. Finally, the CuO_x/MnO_2 heterostructures were obtained and named as the sample M-2. By adjusting the amount of $Cu(AC)_2{\cdot}H_2O$, a series of CuO_x/MnO_2 heterostructures using 0.3 and 0.4 g of $Cu(AC)_2{\cdot}H_2O$ were obtained and denoted as M-3 and M-4, respectively. The synthesis of the CuO_x/MnO_2 heterostructures is shown in **Figure 1**.

2.3. Characterization

X-Ray power diffraction (XRD) patterns were recorded on a Rigaku D/max-2550 PC X-ray power diffractometer employing Cu-K a radiation operating at 40 kV and 200 mA. The morphology of the samples was observed using a field emission scanning electron microscope (SEM, S-4800) at an acceleration voltage of 5

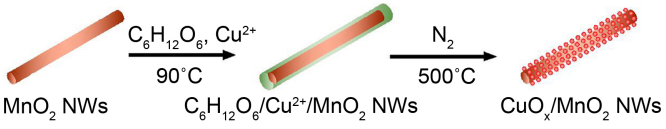

Figure 1. Schematic illustration of the synthesis procedure for CuO_x/MnO_2 heterostructures.

kV. The UV-vis diffuse reflectance spectra (DRS) of the sample were performed on a Perkin Elmer Lambda 35 spectrophotometer, using $BaSO_4$ as reference. The photoluminescence (PL) emission spectra of the samples were obtained using a fluorescence spectrophotometer (FS-5) at room temperature.

2.4. Photocatalyst Activity Texts

The photocatalytic activities of the as-prepared samples were evaluated using the degradation of methylene blue (MB) at room temperature under visible light irradiation. In photocatalytic experiment, 20 mg photocatalysts was suspended in 50 mL of MB solutions (5 $mg \cdot L^{-1}$). Before lighting on, the suspension was stirred for 30 min in the dark to ensure absorption-desorption equilibrium between the photocatalyst and organic dye solution. After that, the suspension under magnetic stirring was placed approximately 20 cm below a xenon lamp (500 W, Model PLS-SXE300) with a cut-off filter that only emits visible light ($\lambda > 400$ nm). At a given time period, the 3 mL suspension was removed from the original solution and centrifuged at 8000 rpm for 3 min to remove the remnant photocatalyst, The absorbance of MB concentration were analyzed by a UV-vis spectrophotometer (UV-2550, Shimadzu) at wavelength 664 nm. After testing, the suspension was returned and the irradiation was resumed. Consequently, the degradation rate for MB could be calculated according to the change of the absorbance.

3. Results and Discussion

3.1. Preparation and Characterization of Catalysts

CuO_x/MnO_2 heterostructures with different amount of $Cu(AC)_2 \cdot H_2O$ (0.2 g, 0.3 g and 0.4 g) were prepared via a simple chemical both and calcination method. MnO_2 NWs were produced by a reaction of $KMnO_4$ and concentrated HCl and then crystallized during the hydrothermal process. Meanwhile Cu^{2+} and glucose were deposited onto the surface of MnO_2 NWs. The conversion of CuO_x from Cu^{2+} was achieved by the subsequent calcination process under N_2 protection. The resulting catalysts are named as M-2, M-3 and M-4, respectively.

The phase of CuO_x/MnO_2 heterostructures was analyzed using the XRD measurements. **Figure 2** presents the XRD patterns of the pure MnO_2 NWs, M-2, M-3 and M-4. In the XRD pattern of the pure MnO_2 NWs, all diffraction peaks at the 2θ values of 12.7˚, 18.0˚, 28.8˚, 37.5˚, 38.8˚, 41.9˚, 49.8˚, 56.1˚, 60.1˚, 65.3˚ and 69.3˚ correspond to the (110), (200), (310), (211), (330), (301), (411), (660), (521), (002) and (541) crystal faces of α-MnO_2 (JCPDS Card No: 44-0141), respectively. No impurity peaks are found within experimental error, indicating a high purity of α-MnO_2. In the XRD pattern of M-2, three characteristic peaks with 2θ values of 32.3˚, 35.8˚ and 57.5˚ are attributed to the (110), (11-1) and (202) crystal planes [27] of CuO (JCPDS Card No: 048-1548), and the peaks with 2θ values of 30.5˚, 37.5˚ and 62.9˚ could be indexed to the (110), (111) and (220) crystal planes of Cu_2O (JCPDS Card No: 78-2076), respectively. The Cu_2O (111)

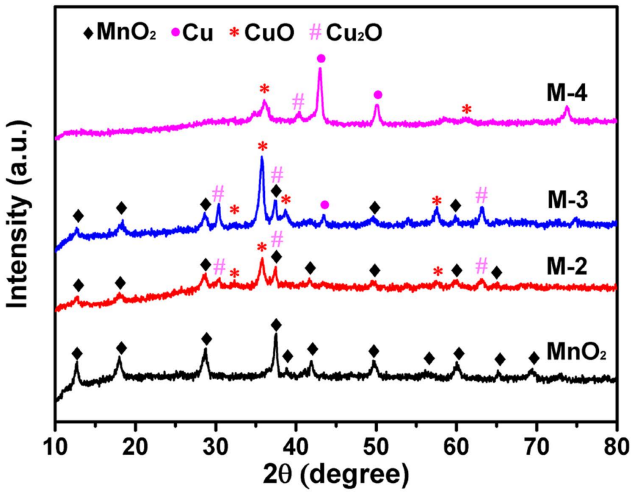

Figure 2. XRD patterns of the pure MnO_2 nanowires, M-2, M-3 and M-4.

peak is very close to the MnO_2 (211) peak and thus they are overlapped at around 37.5 in the pattern, and the other peaks can be indexed to MnO_2. Compared with the pure MnO_2 NWs, the intensity of MnO_2 diffraction peaks obviously decreases in the XRD pattern of M-2. Thus, according to the XRD results, the sample M-2 is consisted of three phases of CuO, Cu_2O and MnO_2, indicating that the information of CuO_x/MnO_2 heterostructures. In the XRD pattern of M-3, we can clearly see that there are four characteristic peaks with 2θ values of 32.3˚, 35.8˚, 38.7˚ and 57.5˚ corresponding to the (110), (111), (11-1) and (202) crystal planes of CuO, respectively, Three peaks with 2θ values of 30.5˚, 37.5˚ and 62.9˚ correspond to the (110), (111) and (220) crystal planes of Cu_2O, and one peak with 2θ value of 43.0˚ is assigned to the (111) crystal planes of Cu (JCPDS Card No: 04-0836) [28], and the other peaks can be indexed to MnO_2. The intensity of MnO_2 diffraction peaks in the XRD pattern of M-3 was weaker than one in the XRD pattern of M-2. According to the XRD results, the sample M-3 is composed of four phases of CuO, Cu_2O, Cu and MnO_2, indicating that the information of CuO_x/MnO_2 heterostructures. In the XRD pattern of M-4, we can also clearly see there are two peaks at around 43.0˚ and 50.1˚ corresponding to the (111) and (200) crystal planes of Cu, and two peaks at around 35.8˚ and 61.2˚ are attributed to the (002) and (113) crystal planes of CuO, and one peak at 40.5˚ is consistent with the (200) crystal planes of Cu_2O. No peaks of MnO_2 are found due to the loading of CuO_x. So the sample M-4 is composed of four phases of CuO, Cu_2O, Cu and MnO_2. The above results verify the formation of CuO_x/MnO_2 heterostructures.

3.2. SEM Images of the Pure MnO_2 NWs, M-2, M-3 and M-4

The morphology of MnO_2 NWs, M-2, M-3 and M-4 was observed in scanning electron microscopy (SEM) images, which are shown in Figure 3. Figure 3(a) and b are the SEM images of the pure MnO_2 NWs with different magnifications.

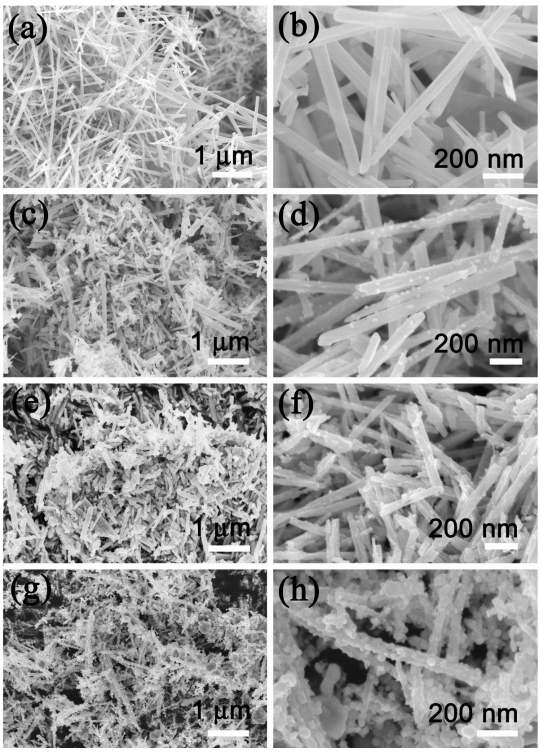

Figure 3. SEM images of the pure MnO_2 nanowires (a)-(b), M-2 (c)-(d), M-3 (e)-(f) and M-4 (g)-(h).

It can be clearly seen that the pure MnO_2 NWs with diameters of about 30 - 80 nm and lengths of 2 - 3 um have a relatively smooth surface, and MnO_2 NWs were uniform in diameter through the entire length and gathered in disorder. As can be seen from **Figure 3(c)** and **Figure 3(d)**, a small and sparse nanoparticles with the sizes of 10 - 20 nm were deposited on the surface of MnO_2 NWs in the sample M-2 prepared using 0.2 g of $Cu(AC)_2{\cdot}H_2O$. When increasing the amount of $Cu(AC)_2{\cdot}H_2O$ to 0.3 g in the sample M-3, as shown in **Figure 3(e)** and **Figure 3(f)**, the sizes of nanoparticles on the surfaces of MnO_2 NWs increase to 20 - 40 nm. Using 0.4 g of $Cu(AC)_2{\cdot}H_2O$ in the sample M-4 (**Figure 3(g)** and **Figure 3(h)**), the bigger and more nanoparticles with diameters of 20 - 50 nm were deposited on the surfaces of MnO_2 NWs, and the surface of MnO_2 NWs is obviously rough. Additionally, it can not be observed the more density of nanoparticles grown on the surface of MnO_2 NWs with increasing the amount of $Cu(AC)_2{\cdot}H_2O$ to 0.5 g. These nanoparticles are considered to be the composite of CuO_x. So, a series of CuO_x/MnO_2 heterostructures of the sample M-2, M-3 and M-4 were successfully fabricated by changing the amount of $Cu(AC)_2{\cdot}H_2O$.

We investigate the optical properties of the pure MnO_2 NWs and CuO_x/MnO_2 heterostructures using a combination of UV-vis and PL technologies. **Figure 4(a)** shows the UV-vis absorbance spectra of the pure MnO_2 NWs and CuO_x/MnO_2 heterostructures (M-2, M-3 and M-4). From the spectra, the characteristic absorption peak of the pure MnO_2 NWs is at 450 nm and the absorption band edge enlarges to almost the full visible region [29]. The sample M-2 and M-3 of

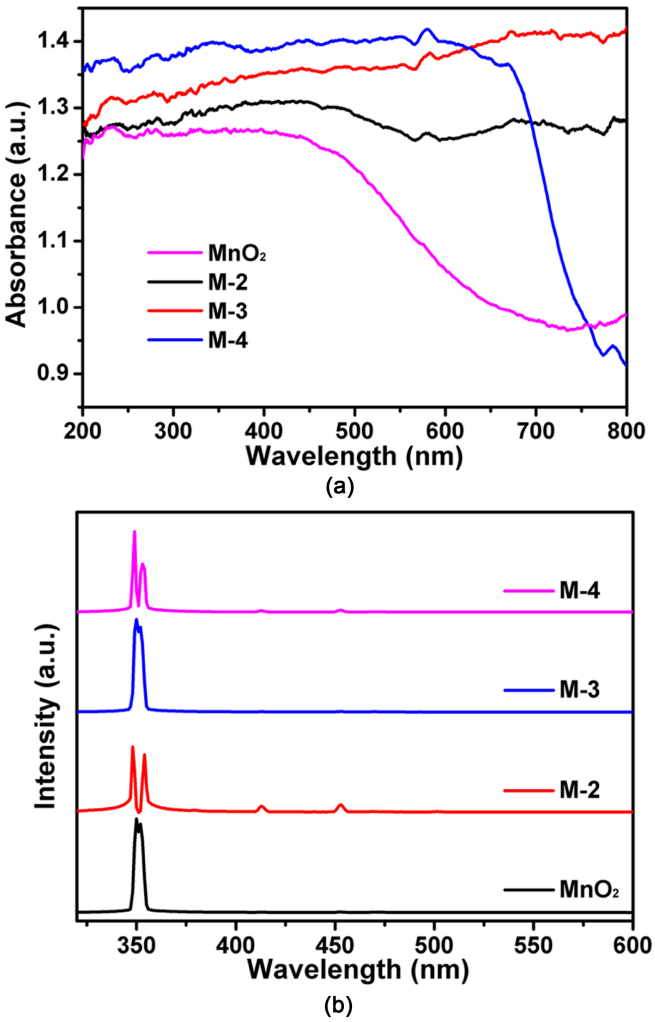

Figure 4. (a) The UV-vis absorption spectra of the pure MnO_2 NWs, M-2, M-3 and M-4, (b) The PL spectra of the pure MnO_2 NWs, M-2, M-3 and M-4.

the CuO_x/MnO_2 heterostructures show two broad bands at 400 - 460 nm and 650 - 700 nm. With the increase of the amount of $Cu(AC)_2{\cdot}H_2O$, the absorption intensity of the sample M-2 and M-3 was enhanced gradually, which further confirms that Cu^{2+} had been successfully anchored on the surface of the MnO_2 NWs. In comparison with the sample M-2 and M-3, the sample M-4 shows a broad and strong absorption in visible light range (400 - 700 nm), and the band gap energy (E_g) of the sample M-4 calculated on the basis of the corresponding absorption edge was 1.57 eV, showing a significant red-shift compared with the pure MnO_2 NWs. It suggested that the sample M-4 might display good photocatalytic activity under visible light.

The photoluminescence (PL) spectra were characterized the trapping, migration and separation of electron-hole pairs, and the lower PL intensity indicates the higher photocatalytic properties of the nanomaterials [30]. The PL spectrum of the samples is measured at room temperature using 300 nm as an excitation

wavelength (**Figure 4(b)**). It is clear that two strong emission peaks of the pure MnO_2 NWs are at about 349 and 351 nm and it is similar to the emission peaks of M-3. Compared with the emission peaks of the pure MnO_2 NWs and M-3, the PL spectra of M-2 and M-4 consist of two weak emission peaks located at about 348 nm and 353 nm and two weaker emission peaks at 412 nm and 453 nm [31] [32]. The sample M-4 among all the samples showed the lowest PL emission intensity and indicated the enhancement of photocatalytic performance.

3.3. Photocatalytic Activity

To evaluate the photocatalytic activity of the as-synthesized CuO_x/MnO_2 heterostructures, the degradation of MB (methylene blue, a standard organic dye) under visible light radiation is utilized as a probe reaction, and displays a characteristic absorption of MB at a wavelength of around 664 nm in absorption spectra. For comparison, the photocatalytic experiment using the pure MnO_2 NWs as the catalyst is also conducted under the same condition. One thing to note here is that before irradiation the mixed solution of the photocatalysts and MB is stirred for 30 min in the dark to establish the adsorption/desorption equilibrium on the photocatalyst surfaces. The corresponding photocatalytic properties have been demonstrated in **Figure 5**. **Figure 5(a)** shows the temporal evolution of the absorption spectra of MB over the sample M-4. The characteristic absorption peak of MB at wavelength of 664 nm decreases sharply as the reaction time increases and almost disappears after 140 min, confirming that MB can be efficiently degraded by the sample M-4. **Figure 5(b)** presents the degradation curves of MB over different catalysts. When using the pure MnO_2 NWs as the photocatalyst, only 47.2% of MB is degraded due to the fast recombination rate of charge carriers, resulting from the narrow band gap [18]. Interestingly, all the CuO_x/MnO_2 heterostructures (M-2, M-3 and M-4) display higher activities than the pure MnO_2 NWs, and the MB degradation efficiencies reach up to 69.3%, 89.2% and 96.1%, respectively. It is obvious that the photocatalytic activity of the pure MnO_2 NWs is improved due to different amount of CuO_x was loaded on the surface of MnO_2 NWs. This may be ascribed to a large specific surface area which can introduce more unsaturated coordination sites in the surface that exposed to MB molecules, that is more favorable for the photocatalytic degradation of MB molecules [33].

In order to better understand the photocatalytic efficiency of the catalysis, the curve of $\ln(C_0/C)$ *versus* time of MB photodegradation process was also investigated. On the basis of the Langmuir-Hinshelwood model, the linear relationship of $\ln(C_0/C)$ *versus* time can be described as: $-\ln(C_0/C) = kt$, where k represents the reaction rate constant of the pseudo-first-order. **Figure 6** shows the effect of different samples on the kinetics of MB under visible light irradiation. The value of apparent rate constant *k*, which is equal to the corresponding slope of the simulation curve, is shown in the inset of **Figure 6** in the form of a histogram graph. It can be seen that the *k* values for the pure MnO_2 NWs, M-2, M-3 and

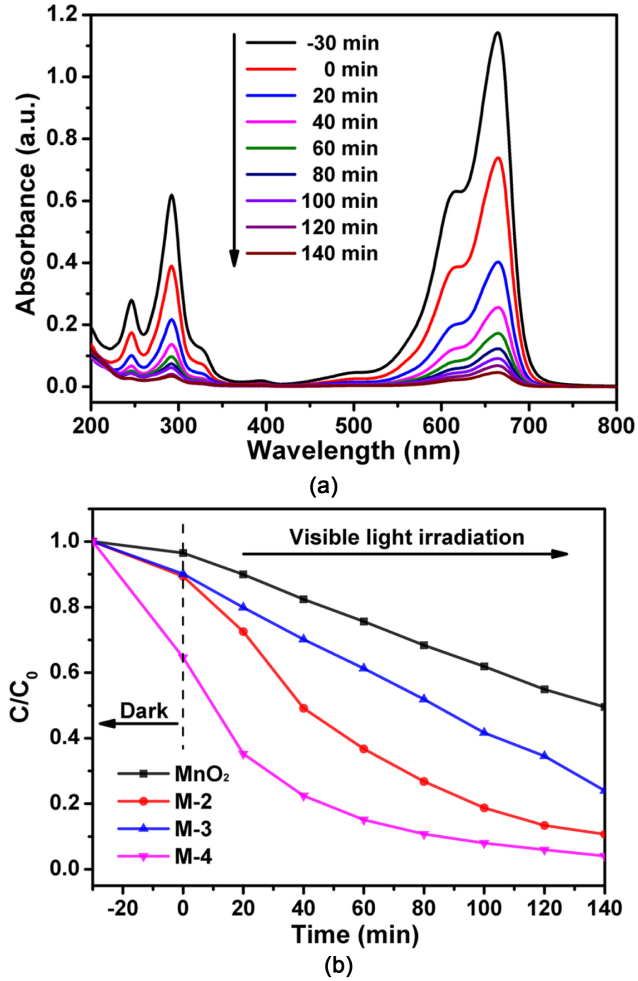

Figure 5. (a) Degradation curves of MB solution over M-4 under visible light, (b) Comparison of photocatalytic activities over the pure MnO_2 NWs, M-2, M-3 and M-4.

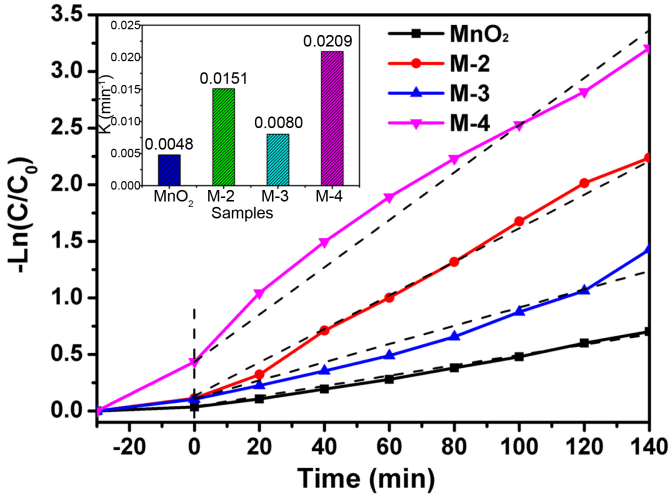

Figure 6. Kinetic linear simulation curves of MB photocatalytic degradation over different samples under visible light irradiation. Inset is the apparent rate constant *k* of each sample.

M-4 are 0.005 min^{-1}, 0.015 min^{-1}, 0.008 min^{-1} and 0.021 min^{-1}, respectively. These results show the introduction of CuO_x improve the visible light photocatalytic performance of the MnO_2 NWs and the sample M-4 exhibits the highest photodegraded efficiency.

The stability and reusability of photocatalysts is another important consideration for their practical applications. Therefore, MB recycling degradation experiments over the sample M-4 were also conducted. Figure 7 shows the degradation efficiencies of MB in three cycles, the first degradation rate of MB was 93.73% and 84.35% for the second time. After repeating the procedure 3 times, the degradation rate still remained at 84.07%, and there is a slight loss of photocatalytic activity, demonstration the good recyclability of M-4. This result indicates that the sample M-4 can still remain stable and efficient during organic dye degradation. Comparing these samples, the sample M-4 has better degradation

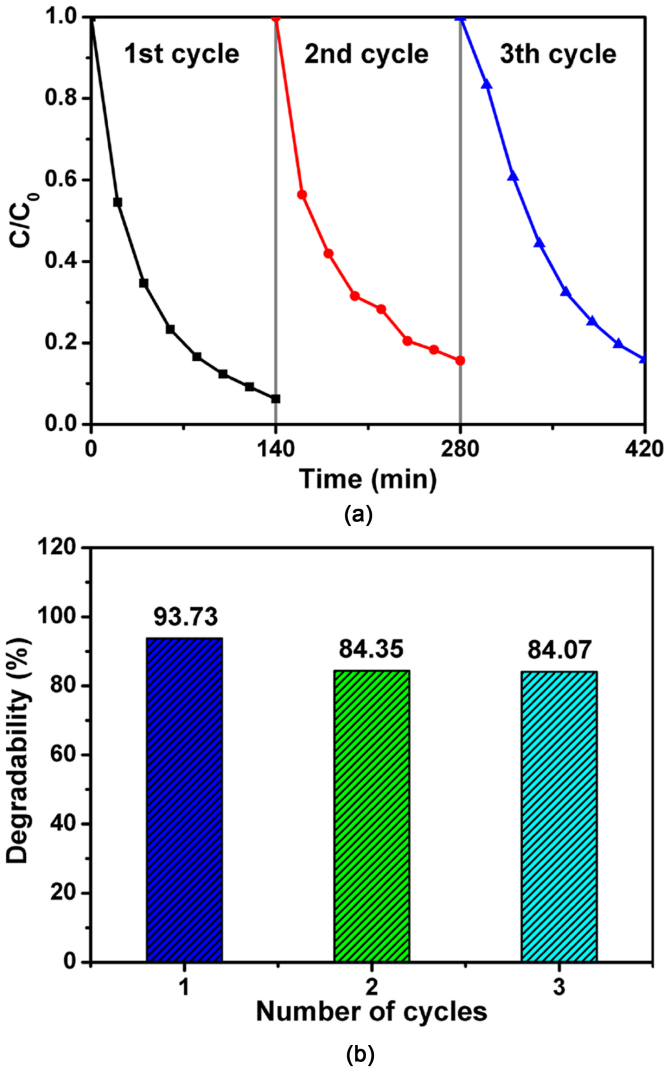

Figure 7. (a) Three cycles of photocatalytic activities of M-4 for the degradation of MB. (b) photocatalytic degradation rate at different recycling times.

activity, which indicates CuO_x nanoparticles on the surface of MnO_2 nanowires played key roles in the enhanced photocatalytic performance. The enhancement may be due to the following reasons. Firstly, the higher photocatalysis efficiency of the heterostructure samples could be explained in terms of the enhancement of UV-vis absorbance spectra and the weaker PL emissions due to CuO_x nanoparticle depositions. Secondly, CuO_x nanoparticles on the surface of CuO_x/MnO_2 heterostructures have the increase of surface area, and inhibit the recombination of electron-hole pairs caused by electronic conduction of Cu nanoparticles [34].

4. Conclusion

In summary, CuO_x/MnO_2 heterostructure photocatalyst was successfully synthesized through a facile and effective hydrothermal method and chemical both/calcination route. For the sample M-2 of CuO_x/MnO_2 heterostructures, CuO_x is composed of two phases of CuO and Cu_2O, and for the sample M-3 and M-4 of CuO_x/MnO_2 heterostructures, CuO_x is consisted of three phases of CuO, Cu_2O and Cu. The sample M-4 in the degradation of MB under visible light showed enhanced photocatalytic activity compared to M-2, M-3 and pure MnO_2 NWs. The enhanced photocatalytic performance can be attributed to the introduction of CuO_x on the surface of MnO_2 NWs and the efficient separation of the electron-hole pairs. The present study thus offers a facile and efficient synthesis method and a promising candidate catalyst for poisonous wastewater treatment in the near future.

Acknowledgements

This research was supported by the Foundation of Shanghai University of Engineering Science (Grant No. 2012gp13, E1-0501-15-0105), Innovation Program of Shanghai Municipal Education Commission (Grant No. 14ZZ160), Open Fund of State Key Laboratory for Modification of Chemical Fibers and Polymer Materials, Donghua University (Grant No. LK1209).

References

[1] Wang, H.L., Zhang, L.S., Chen, Z.G., Hu, J.Q., Li, S.J., Wang, Z.H., Liu, J.S. and Wang, X.C. (2014) Semiconductor Heterojunction Photocatalysts: Design, Construction, and Photocatalytic Performances. *Chemical Society Reviews*, **43**, 5234-5244. https://doi.org/10.1039/C4CS00126E

[2] Liu, Y., Luo, C., Sun, J., Li, H., Sun, Z. and Yan, S. (2015) Enhanced Adsorption Removal of Methyl Orange from Aqueous Solution by Nanostructured Proton-Containing δ-MnO_2. *Journal of Materials Chemistry A*, **3**, 5674-5682. https://doi.org/10.1039/C4TA07112C

[3] Qu, J., Shi, L., He, C., Gao, F., Li, B., Zhou, Q., Hu, H., Shao, G., Wang, X. and Qiu, J. (2014) Highly Efficient Synthesis of Graphene/MnO_2 Hybrids and Their Application for Ultrafast Oxidative Decomposition of Methylene Blue. *Carbon*, **66**, 485-492. https://doi.org/10.1016/j.carbon.2013.09.025

[4] Sang, L.X., Zhao, Y.X. and Burda, C. (2014) TiO_2 Nanoparticles as Functional Building Blocks. *Chemical Reviews*, **114**, 9283-9318.

https://doi.org/10.1021/cr400629p

[5] Chen, X.B., Liu, L., Yu, P.Y. and Mao, S.S. (2011) Increasing Solar Absorption for Photocatalysis with Black Hydrogenated Titanium Dioxide Nanocrystals. *Science*, **331**, 746-750. https://doi.org/10.1126/science.1200448

[6] Marschall, R. (2014) Semiconductor Composites: Strategies for Enhancing Charge Carrier Separation to Improve Photocatalytic Activity. *Advanced Functional Materials*, **24**, 2421-2440. https://doi.org/10.1002/adfm.201303214

[7] Tong, H., Ouyang, S.X., Bi, Y.P., Umezawa, N., Oshikiri, M. and Ye, J.H. (2012) Nano-Photocatalytic Materials: Possibilities and Challenges. *Advanced Materials*, **24**, 229-251. https://doi.org/10.1002/adma.201102752

[8] Zhao, H., Zhang, G. and Zhang, Q. (2014) MnO_2/CeO_2 for Catalytic Ultrasonic Degradation of Methyl Orange. *Ultrasonics Sonochemistry*, **21**, 991-996. https://doi.org/10.1016/j.ultsonch.2013.12.002

[9] Gao, F.Y., Tang, X.L., Yi, H.H., Chu, C., Li, N., Li, J.Y. and Zhao, S.Z. (2017) *In-Situ* DRIFTS for the Mechanistic Studies of NO Oxidation over α-MnO_2, β-MnO_2 and β-MnO_2 Catalysts. *Chemical Engineering Journal*, **322**, 525-537. https://doi.org/10.1016/j.cej.2017.04.006

[10] Li, D.K. and Guo, Z.G. (2017) Stable and Self-Healing Superhydrophobic MnO_2@ Fabrics: Applications in Self-Cleaning, Oil/Water Separation and Wear Resistance. *Journal of Colloid and Interface Science*, **503**, 124-130. https://doi.org/10.1016/j.jcis.2017.05.015

[11] Zhao, D., Yang, X., Zhang, H., Chen, C. and Wang, X. (2010) Effect of Environmental Conditions on Pb (II) Adsorption on β-MnO_2. *Chemical Engineering Journal*, **164**, 49-55.

[12] Singh, M., Thanh, D.N., Ulbrich, P., Strnadová, N. and Stěpánek, F. (2010) Synthesis, Characterization and Study of Arsenate Adsorption from Aqueous Solution by α- and β-Phase Manganese Dioxide Nanoadsorbents. *Journal of Solid State Chemistry*, **183**, 2979-2986.

[13] Wang, Q.F., Xu, J., Wang, X.F., Liu, B., Hou, X.J., Yu, G., Chen, D. and Shen, G.Z. (2014) Core-Shell $CuCo_2O_4$@MnO_2 Nanowires on Carbon Fabrics as High-Performance Materials for Flexible, All-Solid-State, Electrochemical Capacitors. *ChemElectroChem*, **1**, 559-564. https://doi.org/10.1002/celc.201300084

[14] Li, W.Y., Li, G., Sun, J., Zou, R., Xu, K., Sun, Y., Chen, Z., Yang, J. and Hu, J.Q. (2013) Hierarchical Heterostructures of MnO_2 Nanosheets or Nanorods Grown on Au-Coated Co_3O_4 Porous Nanowalls for High-Performance Pseudocapacitance. *Nanoscale*, **5**, 2901-2908. https://doi.org/10.1039/c3nr34140b

[15] Xiao, W., Wang, D. and Lou, X.W. (2010) Shape-Controlled Synthesis of MnO_2 Nanostructures with Enhanced Electrocatalytic Activity for Oxygen Reduction. *The Journal of Physical Chemistry C*, **114**, 1694-1700. https://doi.org/10.1021/jp909386d

[16] Saravanakumar, K., Muthuraj, V. and Vadivel, S. (2016) Constructing Novel Ag Nanoparticles Anchored on MnO_2 Nanowires as an Efficient Visible Light Driven Photocatalyst. *RSC Advances*, **6**, 61357-61366. https://doi.org/10.1039/C6RA10444D

[17] Zheng, X., Han, Z., Yang, W., Qu, F., Liu, B. and Wu, X. (2016) 3D Co_3O_4@MnO_2 Heterostructures Grown on a Flexible Substrate and Their Applications in Supercapacitor Electrodes and Photocatalysts. *Dalton Transactions*, **45**, 16850-16858. https://doi.org/10.1039/C6DT03076A

[18] Liu, S., Liu, H., Jin, G. and Yuan, H. (2015) Preparation of Novel Flower-Like MnO_2/BiOI Composite with Highly Enhanced Adsorption and Photocatalytic Activity. *RSC Advances*, **5**, 45646-45653. https://doi.org/10.1039/C5RA02402A

[19] Dorraj, M., Alizadeh, M., Sairi, N.A., Basirun, W.J., Goh, B.T., Woi, P.M. and Alias, Y. (2017) Enhanced Visible Light Photocatalytic Activity of Copper-Doped Titanium Oxide-Zinc Oxide Heterojunction for Methyl Orange Degradation. *Applied Surface Science*, **414**, 251-261.

[20] Zhang, W.L., Sun, Y.G., Xiao, Z.Y., Li, W.Y., Li, B., Huang, X.J., Liu, X.J. and Hu, J.Q. (2015) Heterostructures of CuS Nanoparticle/ZnO Nanorod Arrays on Carbon Fibers with Improved Visible and Solar Light Photocatalytic Properties. *Journal of Materials Chemistry A*, **3**, 7304-7313. https://doi.org/10.1039/C5TA00560D

[21] Huang, C., Long, Z., Miyauchi, M. and Qiu, X. (2014) A Facile One-Pot Synthesis of Cu-Cu_2O Concave Cube Hybrid Architectures. *CrystEngComm*, **16**, 4967-4972. https://doi.org/10.1039/C4CE00250D

[22] Shi, H., Yu, K., Sun, F. and Zhu, Z. (2012) Controllable Synthesis of Novel Cu_2O Micro/Nano-Crystals and Their Photoluminescence, Photocatalytic and Field Emission Properties. *CrystEngComm*, **14**, 278-285. https://doi.org/10.1039/C1CE05868A

[23] Yin, M., Wu, C.K., Lou, Y., Burda, C., Koberstein, J.T., Zhu, Y. and O'Brien, S. (2015) Copper Oxide Nanocrystals. *Journal of the American Chemical Society*, **127**, 9506-9511. https://doi.org/10.1021/ja050006u

[24] Yu, H., Yu, J., Liu, S. and Mann, S. (2007) Template-Free Hydrothermal Synthesis of CuO/Cu_2O Composite Hollow Microspheres. *Chemistry of Materials*, **19**, 4327-4334. https://doi.org/10.1021/cm070386d

[25] Zhou, B., Liu, Z., Wang, H., Yang, Y. and Su, W. (2009) Experimental Study on Photocatalytic Activity of Cu_2O/Cu Nanocomposites under Visible Light. *Catalysis Letters*, **132**, 75-80. https://doi.org/10.1007/s10562-009-0063-3

[26] Chen, W., Fan, Z. and Lai, Z. (2013) Synthesis of Core-Shell Heterostructured Cu/Cu_2O Nanowires Monitored by *in Situ* XRD as Efficient Visible-Light Photocatalysts. *Journal of Materials Chemistry A*, **1**, 13862-13868. https://doi.org/10.1039/c3ta13413j

[27] Basnet, P. and Zhao, Y.P. (2016) Tuning the Cu_xO Nanorod Composition for Efficient Visible Light Induced Photocatalysis. *Catalysis Science & Technology*, **6**, 2228-2238. https://doi.org/10.1039/C5CY01464F

[28] Zhang, R.R., Hu, L., Bao, S.X., Li, R., Gao, L., Li, R. and Chen, Q.W. (2016) Surface Polarization Enhancement: High Catalytic Performance of Cu/CuO_x/C Nanocomposites Derived from Cu-BTC for CO Oxidation. *Journal of Materials Chemistry A*, **4**, 8412-8420. https://doi.org/10.1039/C6TA01199C

[29] Xue, M., Huang, L., Wang, J.Q., Wang, Y., Gao, L., Zhu, J.H. and Zou, Z.G. (2008) The Direct Synthesis of Mesoporous Structured MnO_2/TiO_2 Nanocomposite: A Novel Visible-Light Active Photocatalyst with Large Pore Size. *Nanotechnology*, **19**, 185604-185611. https://doi.org/10.1088/0957-4484/19/18/185604

[30] Kumar, P.S., Selvakumar, M., Babu, S.G., Jaganathan, S.K., Karuthapandian, S. and Chattopadhyay, S. (2015) Novel CuO/Chitosan Nanocomposite Thin Film: Facile Hand-Picking Recoverable, Efficient and Reusable Heterogeneous Photocatalyst. *RSC Advances*, **5**, 57493-57501. https://doi.org/10.1039/C5RA08783J

[31] Huo, J.P., Fang, L.T., Lei, Y.L., Zeng, G.C. and Zeng, H.P. (2014) Facile Preparation of Yttrium and Aluminum Co-Doped ZnO via a Sol-Gel Route for Photocatalytic Hydrogen Production. *Journal of Materials Chemistry A*, **2**, 11040-11044. https://doi.org/10.1039/C4TA02207F

[32] John, R.E., Chandran, A., Thomas, M., Jose, J. and George, K.C. (2016) Surface-Defect Induced Modifications in the Optical Properties of *α*-MnO Nanorods. *Applied Surface Science*, **367**, 43-51.

[33] Li, H., Yu, K., Lei, X., Guo, B., Li, C., Fu, H. and Zhu, Z. (2015) Synthesis of MoS_2@CuO Heterogeneous Structure with Improved Photocatalysis Performance and H_2O Adsorption Analysis. *Dalton Transactions*, **44**, 10438-10447. https://doi.org/10.1039/C5DT01125F

[34] Yang, J.B., Li, Z., Zhao, C.X., Wang, Y. and Liu, X.Q. (2014) Facile Synthesis of Ag-Cu_2O Composites with Enhanced Photocatalytic Activity. *Materials Research Bulletin*, **60**, 530-536.